

Unconventional pairing in the iron arsenide superconductors

Rafael M. Fernandes, Daniel K. Pratt, Wei Tian, Jerel Zarestky, Andreas Kreyssig, Shibabrata Nandi, Min Gyu Kim, Alex Thaler, Ni Ni, Paul C. Canfield, Robert J. McQueeney, Jörg Schmalian, and Alan I. Goldman
Ames Laboratory, U.S. DOE, and Department of Physics and Astronomy, Iowa State University, Ames, IA 50011, USA
 (Dated: February 4, 2022)

We use magnetic long range order as a tool to probe the Cooper pair wave function in the iron arsenide superconductors. We show theoretically that antiferromagnetism and superconductivity can coexist in these materials only if Cooper pairs form an unconventional, sign-changing state. The observation of coexistence in $\text{Ba}(\text{Fe}_{1-x}\text{Co}_x)_2\text{As}_2$ then demonstrates unconventional pairing in this material. The detailed agreement between theory and neutron diffraction experiments, in particular for the unusual behavior of the magnetic order below T_c , demonstrates the robustness of our conclusions. Our findings strongly suggest that superconductivity is unconventional in all members of the iron arsenide family.

PACS numbers: 74.70.Xa ; 74.20.Rp ; 74.25.Dw

The determination of the mechanism of superconductivity in the recently discovered[1, 2] iron arsenide compounds remains the prime issue in this field, requiring knowledge of the symmetry and of the internal structure of the Cooper pair wave function. A promising candidate for the pairing symmetry is the s^{+-} -state, proposed by electronic theories for superconductivity[3–6], where the Cooper pair wave function changes sign between different sheets of the Fermi surface. In distinction to the case of d -wave pairing[7, 8] in the much studied cuprates, no additional symmetry is broken for s^{+-} -pairing [9], making proposals for the determination of the wave function through interference experiments[10–12] more complex and less conclusive. Important clues about superconductivity in strongly correlated electron systems can, however, be deduced by investigating their phase diagrams and the competition between different phases [13, 14].

The iron arsenide superconductors manifest a rich phase diagram where antiferromagnetic (AFM), tetragonal (Tet), orthorhombic (Ort) and superconducting (SC) order are found in close proximity[15–21]. For some compounds, the transition between AFM and SC is of first order[15–17] with regions of inhomogeneous phase coexistence. However, in $\text{Ba}(\text{Fe}_{1-x}\text{Co}_x)_2\text{As}_2$, experiments[18–26] have established homogeneous coexistence of SC and AFM for intermediate x -values. As the system enters the SC state, the ordered magnetic moment smoothly decreases with decreasing temperature[25, 26], a behavior in sharp contrast to what is known for many conventional superconductors [27], where AFM, associated with localized spins, can easily coexist with SC. This provides strong evidence for the fact that superconductivity and magnetic long-range order compete for the same electrons.

In this Rapid Communication we demonstrate that the Cooper pair wave function in the iron arsenides is revealed via the coexistence and competition between superconductivity and magnetic order. We find that AFM and conventional phonon-mediated SC can not coexist,

while unconventional s^{+-} -pairing is located near the borderline between phase coexistence and mutual exclusion. Therefore, the two phases can coexist only if Cooper pairing is unconventional with a sign-changing pairing wave function, whereas the absence of coexistence in other pnictide superconductors can not be used as evidence for conventional pairing. Our neutron scattering measurements confirm all aspects of our theory, including the novel re-entrance of the non-magnetically ordered phase. These findings strongly suggest that superconductivity is unconventional in all members of the iron arsenide family, given their similar electronic structure and transition temperatures.

Microscopic model: we use a few basic ingredients to describe the main features of the iron arsenides: the electronic structure is characterized by two sets of Fermi surface sheets, a hole pocket around the center of the Brillouin zone and an electron pocket shifted by the ordering vector \mathbf{Q} with Hamiltonian:

$$H = \sum_{\mathbf{p},\sigma,l} \varepsilon_{\mathbf{p},l} \psi_{\mathbf{p}\sigma l}^\dagger \psi_{\mathbf{p}\sigma l} + H_{\text{int}}. \quad (1)$$

We use a circular hole Fermi surface, with $\varepsilon_{\mathbf{p},1} = \varepsilon_{1,0} - p^2/(2m) - \mu$, and an elliptical electron Fermi surface, with $\varepsilon_{\mathbf{p}+\mathbf{Q},2} = -\varepsilon_{2,0} + p_x^2/(2m_x) + p_y^2/(2m_y) - \mu$. For the electron-electron interaction, H_{int} , we include a magnetic electronic interaction I , i.e. $I \sum_{\mathbf{p},\mathbf{p}',\mathbf{q}} \psi_{\mathbf{p}s1}^\dagger \sigma_{ss'} \psi_{\mathbf{p}+\mathbf{q}s'2} \cdot \psi_{\mathbf{p}'s2}^\dagger \sigma_{s's} \psi_{\mathbf{p}'-\mathbf{q}s'1}$ and a pairing interaction $V_{ll'}$, i.e. $\sum_{\mathbf{p},\mathbf{p}',\mathbf{q},ll'} V_{ll'} \psi_{\mathbf{p}+\mathbf{q}\uparrow l}^\dagger \psi_{-\mathbf{p}\downarrow l}^\dagger \psi_{-\mathbf{p}'-\mathbf{q}\downarrow l'} \psi_{\mathbf{p}'\uparrow l'}$. Although our key results are valid for arbitrary pairing matrix $V_{ll'}$, hereafter we will focus on the case of a predominant interband pairing $V_{ll'} = V(1 - \delta_{ll'})$. Depending on the choice for the sign of V , we consider the s^{+-} state, as arising from an electronic pairing mechanism with $V > 0$ [3–6], or the s^{++} state that would result from electron-phonon interaction ($V < 0$). In the latter case, the Cooper pair wave function has the same sign in all Fermi sheets. We analyze the resulting model within a weak coupling mean field theory[28, 29] and obtain the free energy density of a

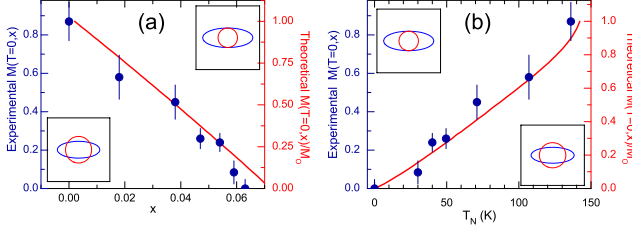


Figure 1: Extrapolated zero temperature ordered moment $M(T=0, x)$ as function of doping x (panel a) and as function of T_N (panel b) for $\text{Ba}(\text{Fe}_{1-x}\text{Co}_x)_2\text{As}_2$. Points correspond to experimental data, whereas the solid line is the result of the calculation described in the text. In the insets, the red circle (blue ellipse) denotes the hole (electron) Fermi pocket.

superconductor with antiferromagnetic long range order:

$$F(\mathbf{M}, \Psi_\alpha) = IM^2 - \frac{V}{2} (\Psi_1^* \Psi_2 + \Psi_2^* \Psi_1) - \frac{T}{N} \sum_{\mathbf{p}, a=\pm} \log \left(4 \cosh \left(\frac{E_{\mathbf{p}a}}{2k_B T} \right) \right). \quad (2)$$

The SC order parameters Ψ_1 and Ψ_2 of the two bands and the staggered moment M are obtained by minimizing $F(\mathbf{M}, \Psi_\alpha)$, where N is the system size and $E_{\mathbf{p}a}$ are the positive eigenvalues of a state with AFM and SC order:

$$E_{\mathbf{p}\pm}^2 = \frac{1}{2} \left(\Gamma_{\mathbf{p}} \pm \sqrt{\Gamma_{\mathbf{p}}^2 + \Omega_{\mathbf{p}} + \delta_{\mathbf{p}}} \right), \quad (3)$$

with $\Gamma_{\mathbf{p}} = 2\Delta_{\text{AFM}}^2 + \Delta_1^2 + \Delta_2^2 + \varepsilon_{\mathbf{p},1}^2 + \varepsilon_{\mathbf{p}+\mathbf{Q},2}^2$ and $\Omega_{\mathbf{p}} = -4(\varepsilon_{\mathbf{p},1}^2 + \Delta_1^2)(\varepsilon_{\mathbf{p}+\mathbf{Q},2}^2 + \Delta_2^2)$ as well as $\delta_{\mathbf{p}} = 8\Delta_{\text{AFM}}^2(\Delta_1\Delta_2 + \varepsilon_{\mathbf{p},1}\varepsilon_{\mathbf{p}+\mathbf{Q},2} - \Delta_{\text{AFM}}^2/2)$. Here $\Delta_l = V\Psi_l$ and $\Delta_{\text{AFM}} = IM$ refer to the SC and AFM single particle gaps.

Neutron diffraction experiments: the neutron diffraction measurements were performed on the HB1A diffractometer at the High Flux Isotope Reactor at Oak Ridge National Laboratory on a series of $\text{Ba}(\text{Fe}_{1-x}\text{Co}_x)_2\text{As}_2$ single crystals using the same spectrometer configuration and data analysis methods described in [25]. The magnetic integrated intensities were determined from rocking scans through the magnetic peak at $\mathbf{Q}_{\text{tet}} = (\frac{1}{2}, \frac{1}{2}, 3)$ as a function of temperature and put on an absolute basis using the known mass of the samples and the magnetic diffraction from the parent compound, BaFe_2As_2 , measured under identical conditions.

The magnetic moment at zero temperature in the absence of SC, $M(T=0, x)$, shown in Fig. 1, was determined by extrapolating the measured order parameter $M(T, x)$ above T_c using a power law fit to the data. The ratios of the integrated intensities of the $(\frac{1}{2}, \frac{1}{2}, 1)$ and $(\frac{1}{2}, \frac{1}{2}, 3)$ magnetic reflections were monitored to ensure that there was no change in the moment direction as a function of temperature and composition x . No additional reflections, e.g. incommensurate magnetic satellites, were observed, in agreement with other work [21].

In Figs. 2a and b, we present a systematic study of the temperature and composition dependence of the magnetic order by neutron diffraction. The key result is shown in Fig. 2b where we see that the magnetic order parameter, for superconducting samples, peaks at T_c and decreases for $T < T_c$. Indeed, for $x = 0.059$, our data show that there is a reentrance of the paramagnetic phase (magnetic long-range order is completely suppressed), in agreement with the predictions of our theory (see below). The opening of the superconducting gap removes states at the Fermi surface that otherwise contribute to the ordered moment, leading to a reduction of the ordered moment below T_c .

Magnetic order in the absence of superconductivity: in Fig. 1, we demonstrate that our model of itinerant magnetism provides a description of the magnetically ordered state that is consistent with the neutron diffraction data. The calculation of $M(T=0, x)$ is done by setting $\Delta_l = 0$, but with magnetic order caused by an electron-electron interaction $I \simeq 0.95$ eV, chosen to yield $T_N = 140$ K at $x = 0$. The other parameters used were $\varepsilon_{1,0} = 0.095$ eV, $\varepsilon_{2,0} = 0.125$ eV, $m = 1.32m_{\text{electron}}$, $m_x = 2m$ and $m_y = 0.3m$, which yield an evolution of the Fermi surface with doping consistent with what is seen by angle resolved photoemission spectroscopy (ARPES) [30]. The suppression of AFM upon doping arises from the detuning of the two Fermi surface sheets; the hole sheet around the Brillouin zone center shrinks and the electron sheet grows upon electron doping (see insets of Fig. 1). The carrier density, x , is fixed under the assumption that each Co adds one electron. This analysis fixes all our parameters, except for the pairing interaction V . The latter is chosen to yield $T_c \simeq 25$ K for x -values where AFM vanishes, yielding $|V| \simeq 0.46$ eV at $x \simeq 0.062$.

Competing order: without AFM order, many properties of s^{++} and s^{+-} pairing states are quite similar. This changes dramatically once AFM and SC compete for the same electrons. For s^{+-} -pairing the excitation energies $E_{\mathbf{p}\pm}$ are fully gapped, whereas for the s^{++} -state nodes occur once $\Delta_{\text{AFM}} > \Delta_1\Delta_2$, at momentum values \mathbf{p}_n given by $E_{\mathbf{p}_n-} = 0$ [31]. This is true even if the nonmagnetic SC state is fully gapped. For the case where $\Delta_1 = \Delta_2$, nodes are located at $\varepsilon_{\mathbf{p}_n,1} = \varepsilon_{\mathbf{p}_n+\mathbf{Q},2}$ (i.e. where Bragg scattering due to AFM is large, see Ref.[31]). Note, however, that in general nodes are not guaranteed to emerge: for example, in the nested case $\varepsilon_{\mathbf{p},1} = -\varepsilon_{\mathbf{p}+\mathbf{Q},2}$ with $I > V$, the s^{++} -state remains fully gapped. To judge whether these AFM-induced nodes for s^{++} -pairing are relevant, one needs to analyze the free energy of Eq.2, which determines whether or not the two phases are allowed to coexist.

In Fig.2 we compare our theoretical results for the phase diagram and the temperature dependence of M^2 with experiments. In Figs. 2c and d we show the calculated phase diagram and the behavior of M^2 for the s^{+-} -state, using the parameters discussed above. The

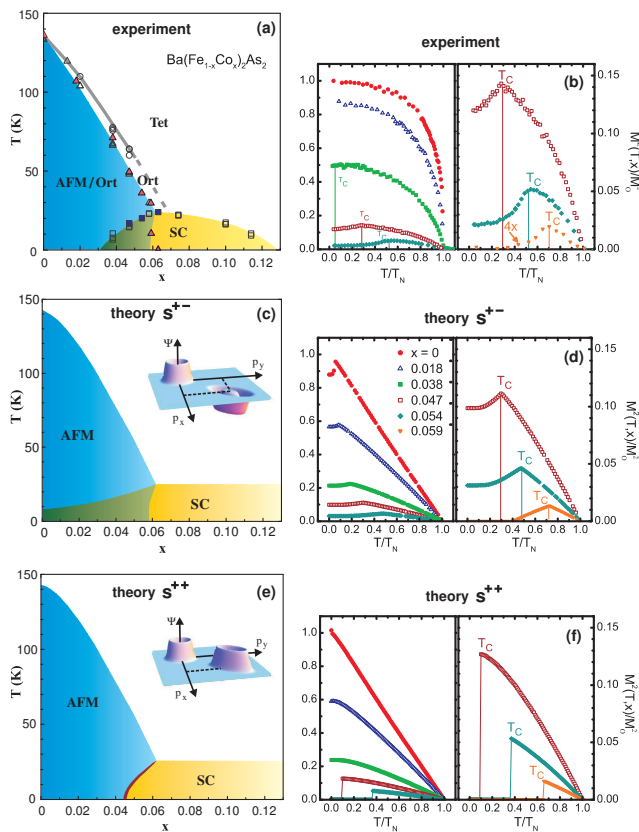


Figure 2: **a**, The phase diagram of $\text{Ba}(\text{Fe}_{1-x}\text{Co}_x)_2\text{As}_2$ determined from neutron diffraction (solid symbols) as well as bulk thermodynamic and transport measurements (open symbols, Ref.[18]). **b**, The AFM order parameter squared measured via neutron diffraction as function of temperature. The right-hand panel shows data in an expanded scale. $M_0 = 0.87\mu_B$ is the ordered moment at $T = x = 0$. **c**, and **d**, The phase diagram and theoretical ordered moment, obtained for an unconventional s^{+-} pairing state (inset). Note the SC and AFM coexistence region, in green. Panels **e** and **f** are analogous to **c** and **d**, but for conventional s^{++} pairing (see inset). Heterogeneous coexistence of AFM and SC regions at the first order transition occurs in panel (e) in a very narrow regime (dark red).

phase coexistence and detailed temperature dependence of the ordered moment agree well with experiment, including the narrow doping regime with reentrance of the AFM transition line. This is clearly different for the s^{++} -state: in Fig.2e and f we show that the two phases can not homogeneously coexist and are separated by a first order phase transition. Thus, s^{+-} -pairing and magnetic order compete but coexist microscopically, whereas both phases are mutually exclusive in case of s^{++} -pairing.

This conclusion is robust and independent of specific details of the model, as follows from a Landau expansion of Eq.2 with respect to the order parameters. This expansion is performed near the multicritical point $T_N = T_c$, where both phase lines meet and where the decision

about coexistence versus mutual exclusion takes place. Figs. 3a, b and c show the Feynman diagrams that are responsible for the order parameters coupling coefficients. The key diagram that is responsible for the different behavior of s^{++} and s^{+-} pairing in Fig.2 is shown in Fig. 3c, corresponding to a term $\mathbf{M}^2(\Psi_1^*\Psi_2 + \Psi_2^*\Psi_1)$ in the energy, which is sensitive to the relative phase, θ , between Ψ_1 and Ψ_2 . Two partners of a Cooper pair in one band are coherently scattered into the other band where they recombine. AFM is essential, as it supplies the momentum transfer \mathbf{Q} needed for the scattering process. While the process contributes to the total energy for either pairing state, the phase of the pair wave-function determines the sign of this contribution, causing the sensitivity of the phase diagram with respect to the internal structure of the Cooper pair wave function.

To illustrate the physical origin (and generality) of our results, we first discuss a simple limit that allows for analytic treatment. Since the low energy electronic structure of the iron pnictides is nearly particle-hole symmetric, we consider $T_N = T_c$ and assume particle-hole symmetry, i.e. $\varepsilon_{\mathbf{p}} \equiv \varepsilon_{\mathbf{p},1} = -\varepsilon_{\mathbf{p}+\mathbf{Q},2}$, implying $\Psi \equiv \Psi_1 = e^{i\theta}\Psi_2$ and $I = |V|$. In this limit, the Landau expansion of Eq.2 (relative to the nonmagnetic normal state) yields:

$$F = \frac{a}{2} (|\Psi|^2 + \mathbf{M}^2) + \frac{u}{4} (|\Psi|^2 + \mathbf{M}^2)^2 + g(\theta) |\Psi|^2 \mathbf{M}^2, \quad (4)$$

which is highly symmetric in the two order parameters. F depends on the phase θ through $g(\theta) = \frac{u}{2}(1 + \cos\theta)$, and on the two coefficients $a = 2I - \frac{I^2}{N} \sum_{\mathbf{p}} \tanh(\frac{\varepsilon_{\mathbf{p}}}{2T}) / \varepsilon_{\mathbf{p}}$

$$\text{and } u = \frac{I^4}{4NT} \sum_{\mathbf{p}} \text{sech}^2(\frac{\varepsilon_{\mathbf{p}}}{2T}) [T \sinh(\frac{\varepsilon_{\mathbf{p}}}{T}) - \varepsilon_{\mathbf{p}}] / \varepsilon_{\mathbf{p}}^3 > 0.$$

Therefore, the following results are completely independent of further details of the band structure dispersion, allowing us to draw general conclusions about the phase diagram for different microscopic pairing states.

If $g > 0$, the two ordered states are separated by a first order transition, while homogeneous phase coexistence and second order transitions only occur if $g < 0$. The s^{++} state, with $g_{++} \equiv g(\theta = 0) = u$, is deep in the first order transition regime. Interestingly, for particle-hole symmetry, the s^{+-} state, with $g_{+-} \equiv g(\theta = \pi) = 0$, is at the border between regimes of coexistence and exclusion. The special symmetry in Eq.4 at $g = 0$ is directly related to the emergent $\text{SO}(6)$ symmetry that was found in electronic theories for s^{+-} pairing[5], as discussed in Ref.[32], suggesting that this result holds beyond weak-coupling. This demonstrates that, for the pnictides, s^{+-} -SC is compatible with AFM, while magnetic order enforces new gap-nodes or strongly reduces the gap for s^{++} -pairing[31], impeding phase coexistence. It is also interesting to note the connection of expression (4) with the $\text{SO}(5)$ model proposed for the cuprates [14].

Now, moving away from the special case of particle-hole symmetry, we note that the inclusion of an infinites-

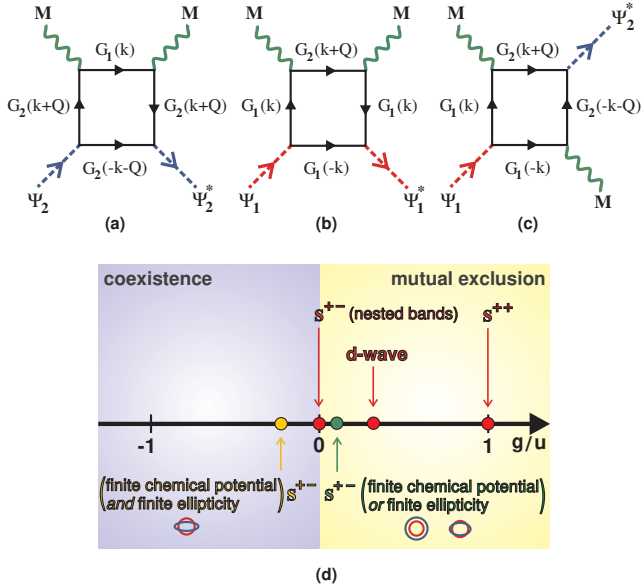


Figure 3: **a**, **b**, and **c**, Feynman diagrams responsible for the coupling coefficients between the SC and AFM order parameters. $G_i(k)$ denotes the non-interacting single particle Green's function. Note that diagram **c** is sensitive to the relative phase between Ψ_1 and Ψ_2 . **d**, Summary of the results for the coupling coefficient g , considering different band dispersions.

imal chemical potential μ or a small ellipticity brings g_{+-} to small but positive values. However, when both the ellipticity and μ are finite, g_{+-} can be negative. Using the parameters that lead to good agreement with the experimental results in Figs. 1 and 2, we find virtually the same result as before for s^{++} , $\frac{g_{++}}{u} \approx 1$, while for s^{+-} the coefficient assumes a negative value, $\frac{g_{+-}}{u} \approx -0.26$, allowing for the phase coexistence presented in Fig. 1.

We note that, for a d -wave state at particle-hole symmetry, we obtain $\frac{g}{u} = \sqrt{\frac{2}{3}} - \frac{1}{2}$, i.e. it is less compatible with AFM than the s^{+-} state. A similar result is obtained for the case of a nodal s^{+-} state. Even though our neutron diffraction measurements did not detect any incommensurability, we checked that our main results still hold even for a small incommensurability. Furthermore, an extension of our model including the lattice degrees of freedom satisfactory describes the behavior of the orthorhombic state below T_c , as we show in [33].

The fact that the s^{+-} state is on the verge of coexistence and mutual exclusion with magnetism implies that the observation of different phase diagrams, with and without coexistence[15–20], does not imply different pairing states. There are situations where the s^{+-} state coexists with AFM, as in $\text{Ba}(\text{Fe}_{1-x}\text{Co}_x)_2\text{As}_2$, and others where it does not - as, for example, in the case of two detuned circular bands [29] (see Fig. 3d). Thus, the presence of a first order transition does not imply s^{++} -

pairing, whereas the inverse is true: observing phase coexistence in the iron arsenides disallows s^{++} SC. This makes $\text{Ba}(\text{Fe}_{1-x}\text{Co}_x)_2\text{As}_2$ a crucially important member of the pnictide family.

We thank Alfred Kracher for performing the WDS measurements and Sergey Bud'ko for assistance with the thermodynamic and transport measurements. This work was supported by the U.S. DOE, Office of BES, DMSE. Ames Laboratory is operated for the U.S. DOE by Iowa State University under Contract No. DE-AC02-07CH11358.

-
- [1] Y. Kamihara *et al.*, J. Am. Chem. Soc. **130**, 3296 (2008).
 - [2] M. Rotter, M. Tegel, and D. Johrendt, Phys. Rev. Lett. **101**, 107006 (2008).
 - [3] I. I. Mazin, D. J. Singh, M. D. Johannes and M. H. Du, Phys. Rev. Lett. **101**, 057003 (2008).
 - [4] K. Kuroki *et al.*, Phys. Rev. Lett. **101**, 087004 (2008).
 - [5] A.V. Chubukov, D. V. Efremov, and I. Eremin, Phys. Rev. B **78**, 134512 (2008).
 - [6] I. I. Mazin and J. Schmalian, Physica C **469**, 614 (2009).
 - [7] D. J. Van Harlingen, Rev. Mod. Phys. **67**, 515 (1995).
 - [8] C. C. Tsuei and J. R. Kirtley, Rev. Mod. Phys. **72**, 969 (2000).
 - [9] V. Stanev, J. Kang, and Z. Tesanovic Phys. Rev. B **78**, 184509 (2008).
 - [10] D. Parker and I. I. Mazin, Phys. Rev. Lett. **102**, 227007 (2009).
 - [11] J. Wu and P. Phillips, Phys. Rev. B **79**, 092502 (2009).
 - [12] J. Linder, I. B. Sperstad, and A. Sudbo, Phys. Rev. B **80**, 020503(R) (2009).
 - [13] Y. Zhang, E. Demler, and S. Sachdev, Phys. Rev. B **66**, 094501 (2002); S. Sachdev, Phys. Status Solid B **247**, 537 (2010).
 - [14] S.-C. Zhang, Science **275**, 1089 (1997).
 - [15] H. Luetkens *et al.*, Nature Mater. **8**, 305 (2009).
 - [16] J. T. Park *et al.*, Phys. Rev. Lett. **102**, 117006 (2009).
 - [17] T. Goko *et al.*, Phys. Rev. B **80**, 024508 (2009).
 - [18] N. Ni *et al.*, Phys. Rev. B **78**, 214515 (2008).
 - [19] J.-H. Chu, J. G. Analytis, C. Kucharczyk, and I. R. Fisher, Phys. Rev. B **79**, 014506 (2009).
 - [20] F. Ning *et al.*, J. Phys. Soc. Jpn. **78** 013711 (2009).
 - [21] C. Lester *et al.*, Phys. Rev. B **79**, 144523 (2009).
 - [22] Y. Laplace, J. Bobroff, F. Rullier-Albenque, D. Colson, and A. Forget, Phys. Rev. B **80**, 140501(R) (2009).
 - [23] M. -H. Julien *et al.*, Europhys. Lett. **87** 37001 (2009).
 - [24] C. Bernhard *et al.*, New J. Phys. **11**, 055050 (2009).
 - [25] D. K. Pratt *et al.*, Phys. Rev. Lett. **103**, 087001 (2009).
 - [26] A. D. Christianson *et al.*, Phys. Rev. Lett. **103**, 087002 (2009).
 - [27] W. Baltensperger and S. Strassler, Phys. Kondens. Mater. **1**, 20 (1963).
 - [28] M. Kato and K. Machida, Phys. Rev. B **37**, 1510 (1988).
 - [29] A. B. Vorontsov, M. G. Vavilov, and A. V. Chubukov, Phys. Rev. B **79**, 060508(R) (2009).
 - [30] C. Liu *et al.*, arXiv:0910.1799 (2009).
 - [31] D. Parker, M. G. Vavilov, A. V. Chubukov, and I. I. Mazin, Phys. Rev. B **80**, 100508(R) (2009).
 - [32] D. Podolsky, H.-Y. Kee, and Y. B. Kim, Europhys. Lett.

88, 17004 (2009).

[33] S. Nandi *et al.*, Phys. Rev. Lett. **104**, 057006 (2010).